

Extensive metabolic cross-talk in melon fruit revealed by spatial and developmental combinatorial metabolomics

Annick Moing^{1,2}, Asaph Aharoni³, Benoit Biais¹, Ilana Rogachev³, Sagit Meir³, Leonid Brodsky³, J. William Allwood⁴, Alexander Erban⁵, Warwick B. Dunn^{4,6}, Lorraine Kay⁷, Sjaak de Koning⁸, Ric C. H. de Vos^{9,10,11}, Harry Jonker^{9,11}, Roland Mumm^{9,11}, Catherine Deborde^{1,2}, Michael Maucourt^{2,12}, Stéphane Bernillon^{1,2}, Yves Gibon^{1,2}, Thomas H. Hansen¹³, Søren Husted¹³, Royston Goodacre^{4,6}, Joachim Kopka⁵, Jan K. Schjoerring¹³, Dominique Rolin¹² and Robert D. Hall^{9,10,11}

¹INRA – UMR 619 Biologie du Fruit, Centre INRA de Bordeaux, F-33140 Villenave d'Ornon, France; ²Metabolome-Fluxome Facility of Bordeaux Functional Genomics Center, IFR103 BVI, Centre INRA de Bordeaux, F-33140 Villenave d'Ornon, France; ³Department of Plant Sciences, Weizmann Institute of Science, POB 26, Rehovot 76100, Israel; ⁴School of Chemistry, Manchester Interdisciplinary Biocentre, 131 Princess Street, Manchester M1 7DN, UK; ⁵MPI Max-Planck-Institute of Molecular Plant Physiology, Am Muehlenberg 1, 14476 Golm, Germany; ⁶Manchester Centre for Integrative Systems Biology, Manchester Interdisciplinary Biocentre, 131 Princess Street, Manchester M1 7DN, UK; ⁷LECO Instruments UK, Hazel Grove, Manchester SK7 5DA, UK; ⁸LECO Instruments, Marie-Bernays-Ring 31, 41199 Mönchengladbach, Germany; ⁹Plant Research International, PO Box 16, 6700 AA Wageningen, the Netherlands; ¹⁰Netherlands Metabolomics Centre, Einsteinweg 55, 2333 CC Leiden, the Netherlands; ¹¹Centre for BioSystems Genomics, PO Box 98, 6700AB, Wageningen, the Netherlands; ¹²Université de Bordeaux, UMR 619 Biologie du Fruit, F-33140 Villenave d'Ornon, France; ¹³Plant and Soil Science Laboratory, Department of Agriculture and Ecology, Faculty of Life Sciences, University of Copenhagen, DK-1871 Frederiksberg C, Copenhagen, Denmark

Summary

Author for correspondence:

Annick Moing

Tel: +33 5 57 12 25 28

Email: moing@bordeaux.inra.fr

Received: 26 October 2010

Accepted: 7 December 2010

New Phytologist (2011)

doi: 10.1111/j.1469-8137.2010.03626.x

Key words: *Cucumis melo* (melon), fruit metabolism, fruit metabolome, fruit quality, mass spectrometry (MS), metabolic profiling, nuclear magnetic resonance (NMR).

- Variations in tissue development and spatial composition have a major impact on the nutritional and organoleptic qualities of ripe fleshy fruit, including melon (*Cucumis melo*). To gain a deeper insight into the mechanisms involved in these changes, we identified key metabolites for rational food quality design.
- The metabolome, volatiles and mineral elements were profiled employing an unprecedented range of complementary analytical technologies. Fruits were followed at a number of time points during the final ripening process and tissues were collected across the fruit flesh from rind to seed cavity. Approximately 2000 metabolite signatures and 15 mineral elements were determined in an assessment of temporal and spatial melon fruit development.
- This study design enabled the identification of: coregulated hubs (including aspartic acid, 2-isopropylmalic acid, β -carotene, phytoene and dihydropseudoionone) in metabolic association networks; global patterns of coordinated compositional changes; and links of primary and secondary metabolism to key mineral and volatile fruit complements.
- The results reveal the extent of metabolic interactions relevant to ripe fruit quality and thus have enabled the identification of essential candidate metabolites for the high-throughput screening of melon breeding populations for targeted breeding programmes aimed at nutrition and flavour improvement.

Introduction

Melon (*Cucumis melo*) is a global crop of high economic importance. It has considerable relevance to the 'five a day' healthy diet regime in providing key nutrients, such as

isoprenoids, vitamins and minerals (Lester, 2008). The most important properties of melons for consumer acceptance are amount of sugar and aroma (Lester, 2008). So far, these traits have been investigated in isolation. For example, sugar metabolism of cantaloupe melon species has been

extensively studied (Burger & Schaffer, 2007). These orange-fleshed melons also accumulate beneficial carotenoids (Cuevas *et al.*, 2008) and their aroma profile has been analysed (Beaulieu & Grimm, 2001; Obando-Ulloa *et al.*, 2008). Moreover, the importance of macroelements for fruit physiology has been recognized; for example, the interaction of potassium (K) with fruit acidity and osmotic potential in relation to growth (Davies *et al.*, 2006), the involvement of calcium (Ca) in cell wall synthesis and signalling (White & Broadley, 2003) and shelf-life (Martin-Diana *et al.*, 2007).

The organoleptic and nutritional qualities of a fleshy fruit are related not only to total metabolite and mineral composition at maturity, but also to developmental and spatial aspects. Melon fruit development is a complex, integrated biological process. However, two general phases have been recognized: early development, characterized by tight spatial and temporal regulation of cell division and cell expansion; and, subsequently, the fruit ripening phase, characterized by important nutritional changes, including taste, flavour and texture (Gillaspy *et al.*, 1993).

So far, little is known about the metabolic interactions between, for example, food aroma compounds and nutritionally relevant macroelements and, specifically, microelements in fleshy fruits. Owing to this lack of information on associations between, for example, primary or secondary metabolism and volatiles or minerals, breeding for fruit quality is currently primarily focused on single quality traits. However, the continued development of metabolomic approaches (Fiehn *et al.*, 2000; Hirai *et al.*, 2007; Bedair & Sumner, 2008) for crop and food product applications has created new opportunities for the discovery of metabolites and metabolic associations highly correlated with food quality traits (Hall *et al.*, 2008; Fernie & Schauer, 2009). Such investigations, especially when performed with the highest possible coverage, appear promising in view of the knowledge gained, as already demonstrated for different fruit species. Such studies employed nontargeted metabolic profiling approaches but were restricted to one or, at most, two analytical platforms (Aharoni *et al.*, 2002; Carrari *et al.*, 2006; Mounet *et al.*, 2007, 2009; Fait *et al.*, 2008; Hanhineva *et al.*, 2008; Mintz-Oron *et al.*, 2008).

In a preliminary study on ripe melon fruit (Biais *et al.*, 2009), quantitative proton NMR spectroscopy ($^1\text{H-NMR}$) of polar extracts highlighted the major metabolites in the flesh of ripe fruit, including sugars, organic acids and amino acids. Their spatial localization was determined using direct $^1\text{H-NMR}$ profiling of juice and gas chromatography coupled with mass spectrometry (GC-MS) profiling of tissue extracts which revealed several gradients of metabolites. A similar approach with different analytical strategies was in agreement with the later work for sugars but also revealed gradients across the ripe fruit flesh for minerals and phyto-

nutrients, including β -carotene, ascorbic acid and folic acid (Lester, 2008).

In the present work, we applied an unprecedented range of complementary metabolomic profiling platforms, including $^1\text{H-NMR}$, liquid chromatography coupled to photodiode array and fluorescence detection (HPLC-PDA-FL), diverse GC-MS and LC-MS screenings, and a macro- and microelement screening by inductively coupled plasma mass spectrometry (ICP-MS) in order to study the spatial and developmental dynamics of melon fruit ripening. The combined data were analysed using unsupervised multivariate analysis to highlight sample similarities and dissimilarities, and clustering (Kerr *et al.*, 2008) and correlation network (Nikiforova & Willmitzer, 2007) approaches to visualize interanalyte relationships. This represents the most comprehensive screening for metabolic patterning and intermetabolite associations in a fruit crop, and also demonstrates how far we have come with multivariate, multiplatform integrated metabolomics.

Following previous assessments of the metabolically important determinants of ripe melon fruit metabolism (Biais *et al.*, 2009, 2010), we discovered novel metabolite patterns relevant to spatial and developmental gradients in melon fruit. Furthermore, taking the melon fruit as a generic example, we demonstrate an effective data mining and discovery strategy, from the raw metabolite and mineral profiles to identification of spatial and developmental patterns and, ultimately, to the investigation of metabolite and mineral associations. These coregulation networks, defined by highly associated metabolites, the so-called 'hubs', are discussed as potential targets for future high-throughput screening of breeding populations. Such 'hub' metabolites are potentially important, robust quality indicators complementing conventional assessment of nutritionally relevant metabolites for breeding processes supported by metabolomics.

Materials and Methods

Melon growth and sample handling

The melon (*Cucumis melo* L.) variety studied was 'Escrito', grown in an open field (9200 plants ha^{-1}) in France (Moissac) between April and August 2008. Plant culture was performed according to standard commercial practices. Melons were harvested at three stages of development. Stage 1 corresponds to developing fruit just before the appearance of the suberized net on the skin, stage 2 to early ripening and stage 3 to ripe fruit at the beginning of abscission (commercial maturity). For each stage, nine melons were selected to make three homogeneous lots (biological replicates) of three fruits each. Two slices of 1 cm thickness were cut in the equatorial plane of each fruit of these three-fruit biological lots. The skin and seeds were removed and five concentric



Fig. 1 Melon sample preparation. Preparation of the samples of flesh in an equatorial disk of fruit.

mesocarp rings of flesh (7 ± 1 mm width) were taken from the periphery (outer mesocarp) to the centre (inner mesocarp) (Fig. 1). The flesh rings of a given position taken from a given three-fruit lot were pooled and immediately deep-frozen and stored at -80°C until grinding in liquid nitrogen (ball grinder, Danguomeau, Clermont-Ferrand, France). The 45 powdered samples (three stages \times three biological replicates \times five flesh positions) were stored at -80°C , aliquoted and transported using dry ice to the different laboratories for fresh-frozen metabolome analyses or were lyophilized for NMR and elemental profiling. In parallel, dry matter content was determined using *c.* 250 mg FW powder aliquots and a 70°C oven.

Chemicals

For NMR analysis, Methanol- d_4 (99.8%) was purchased from Eurisotop (Gif sur Yvette, France) and (trimethylsilyl)propionic-2,2,3,3- d_4 (TSP) acid (98%) from Aldrich (Saint Quentin Fallavier, France). For GC-MS analysis, the Manchester Interdisciplinary Biocentre obtained succinic- d_4 acid, glycine- d_5 , and malonic- d_2 acid standard metabolites (all of 99% purity or greater), high-performance liquid chromatography (HPLC)-grade methanol and water, chloroform, pyridine, *O*-methylhydroxylamine chloride, *N*-acetyl-*N*-(trimethylsilyl)-trifluoroacetamide, and *n*-alkanes (C10, C12, C15, C19, C22) from Sigma-Aldrich (Gillingham, UK). L. K. and S. de K. obtained *O*-methylhydroxylamine chloride and *n*-alkanes (C10, C12, C15, C19, C22, C28, C32, C36) from Sigma-Aldrich (Deisenhofen, Germany), *N*-acetyl-*N*-(trimethylsilyl)-trifluoroacetamide from Macherey-Nagel (Düren, Germany), and pyridine from Merck (Darmstadt, Germany).

NMR analysis of polar compounds

For NMR analysis, polar metabolites were extracted using a hot ethanol/water series, and then analysed, identified and quantified by $^1\text{H-NMR}$ as previously described (Mounet *et al.*, 2007; Biais *et al.*, 2009). For the preparation of extracts and NMR acquisition parameters, special care was taken to allow absolute quantification of individual metabolites through addition of EDTA sodium salt solution to

improve the resolution and quantification of organic acids such as malic and citric acids, and adequate choice of the NMR acquisition parameters. Quantitative $^1\text{H-NMR}$ spectra were recorded at 500.162 MHz and 300 K on a Bruker Avance spectrometer (Wissembourg, France) with a 5 mm inverse probe using a 90° pulse angle and an electronic reference for quantification. Two technological replicates were extracted and analysed for each biological replicate. For organic acid quantification, the sums of the acid and salt forms present in the flesh samples were expressed in mg equivalent of the acid form. Four unknown metabolites, named using the mid-value of the chemical shift and the multiplicity of the corresponding resonance group, were quantified in arbitrary units. The $^1\text{H-NMR}$ spectra of all stages and flesh sections were converted into JCAMP-DX (the Joint Committee on Atomic and Molecular Physical data – Data Exchange format) standard exchange format and have been deposited, with associated metadata and compound list, into the Metabolomics Repository of Bordeaux MeRy-B (<http://www.cbib.u-bordeaux2.fr/MERYB/public/PublicREF.php?REF=M08002>).

GC-MS of polar compounds

The extraction procedure precisely followed that of Biais *et al.* (2009), adapted from Fiehn *et al.* (2000) and Liscic *et al.* (2006). Before derivatization, samples were placed in a speed vacuum concentrator for 30 min to remove residual moisture. Samples were derivatized and supplemented with an *n*-alkane retention index following the [L3] method of Allwood *et al.* (2009). The sample GC-MS analysis with electron impact ionization and time-of-flight (TOF) detection was performed in three ways: first, according to the [L3] method of Allwood *et al.* (2009) using a higher polarity Supelco (Gillingham, UK) SPB-50 (DB17) column, and then according to the [L2] method of Allwood *et al.* (2009) (identical to [L3] other than for the use of a Varian (Oxford, UK) VF4 column) with and without employing a 1 : 100 split injection. The chromatograms were baseline-corrected in LECO (Leco Corp., St. Joseph, MA, USA) ChromaTOF 2.22 and deposited with associated metadata in NetCDF (network Common Data Form) format into MeRy-B (<http://www.cbib.u-bordeaux2.fr/MERYB/public/PublicREF>).

php?REF=M08002). The normalized data were next aligned, mass features extracted, and correlating mass features placed into cluster and time groups using TagFinder (Luedemann *et al.*, 2008) following the [M1] method of Allwood *et al.*, (2009). Peak heights of mass (m/z) fragments were normalized to the succinic-*d4* acid standard. Peak annotation was manually supervised using TagFinder visualizations for mass spectral matching (Luedemann *et al.*, 2008; Allwood *et al.*, 2009). Identification afforded a minimum of three correlating fragments in a cluster or time group and < 5% time deviation from the expected retention index (RI) within the Golm Metabolome Database (<http://csbdb.mpimp-golm.mpg.de/csbdb/gmd/gmd.html>) (Kopka *et al.*, 2005; Strehmel *et al.*, 2008; Hummel *et al.*, 2010). The majority of metabolites detected by GC-MS taken forward to statistical analysis were selected from the [L2] method data set acquired in splitless mode, with the exception of the high-concentration saccharides that were selected from the [L2] split mode data set.

HPLC analysis of lipophilic isoprenoids

Isoprenoids were extracted from 500 mg FW of frozen melon powder and analysed by HPLC (Bino *et al.*, 2005). Compounds were quantified using commercially available standards, or expressed as area per unit of FW. Values below detection limit were randomized between 0 and the detection limit.

Nontargeted liquid chromatography quadrupole time-of-flight tandem mass spectrometry (LC-QTOF-MS) profiling of semipolar compounds

Frozen melon tissues (500 mg FW) were extracted in methanol containing 0.1% formic acid, as described previously (Mintz-Oron *et al.*, 2008) with modifications: following centrifugation, 1 ml of the supernatant was freeze-dried and resuspended in 150 μ l of extraction solvent, for sample concentrating. Samples were injected into a UPLC-QTOF-MS (HDMS-Synapt, Waters, Manchester, UK) (Mintz-Oron *et al.*, 2008). A mixture of 15 standard compounds, injected after each 10 samples, was used for quality control. XCMS (Smith *et al.*, 2006) peak picking/alignment was performed for the negative mode data. The \log_e -transformed and intrareplicate-group normalized intensity profiles of mass signals across samples were recursively clustered based on the Pearson correlation between profiles. Each tightly interconnected cluster was interpreted as a group of fragments, isotopes and adducts of one molecule. The profile of pseudomolecular ion (or a profile of the fragment of the highest intensity) was taken as the profile representative of the cluster (metabolite). The clustering of 2462 mass signals obtained by XCMS resulted in 1246

clusters (metabolites). Metabolites were putatively identified (Supporting Information, Table S1) as described previously (Mintz-Oron *et al.*, 2008).

Nontargeted GC-MS analysis of volatile compounds

Volatile compounds were trapped using headspace solid-phase microextraction (SPME) with a PDMS-DVB fibre (Supelco, Bellefonte, PA, USA) and analysed using an untargeted GC-MS-based metabolomics approach (Tikunov *et al.*, 2005) adapted for melon (Verhoeven *et al.*, 2011). MetAlign software (Lommen, 2009) was used to extract and align all 21 819 mass signals (signal to noise ratio $s/n \geq 3$). Absent values were randomized between 0.1 and three times the noise. The dataset was then filtered for 16 271 reproducible signals (signal intensity of ≥ 100 in \geq three samples); signal redundancy per metabolite was removed by means of clustering and mass spectra were reconstructed (Tikunov *et al.*, 2005). This resulted in 499 volatile compounds represented by at least four masses. Metabolites were putatively identified by matching the mass spectra of obtained metabolites to the NIST 05 (National Institute of Standards and Technology, Gaithersburgh, MD, USA) and Wiley spectral libraries and by comparison with retention indices (calculated using a series of alkanes and fitted with a third-order polynomial function; Strehmel *et al.*, 2008) in the literature. Library hits were manually checked in the raw data, and a series of commercial standards were used to check annotations (Table S2).

Elemental profiling

Freeze-dried melon samples (200–250 mg) were digested in 100 ml closed vessels in a microwave oven (Multiwave 3000; Anton Paar, Graz, Austria) for 50 min at 210°C with a maximum pressure of 40 bar. The digestion medium consisted of 5 ml 65% HNO₃ and 5 ml 15% H₂O₂ (Hansen *et al.*, 2009). After digestion, the samples were diluted to 3.5% HNO₃. Multi-elemental analysis was performed using ICP-MS (Agilent 7500ce; Agilent Technologies, Wokingham, UK) tuned in standard mode. The plasma power was operated at 1450 \pm 50 W and the argon carrier and make-up gases were set at 0.83 and 0.17 l min⁻¹, respectively. Sample uptake was maintained at *c.* 0.1 ml min⁻¹ by a self-aspirating perfluoroalkoxy micro-flow nebulizer (Agilent Technologies, Wokingham, UK). Elimination of spectral interferences was obtained by the use of an octopole ion guide with the cell gases helium or hydrogen (Laursen *et al.*, 2009). For the series of 45 melon samples, seven replicates of certified reference material NIST 1515 (apple leaves, particle size < 75 μ m) were included. Only data deviating < \pm 10% from the certified reference values were retained.

Statistical analysis

A two-factor ANOVA was performed using Multi Experiment Viewer software (MeV), version 4.2 (Saeed *et al.*, 2003) on \log_e -transformed data to determine the analytes that were retained for further analyses. Then, to explore the analyte multidimensional data set, principal component analysis (PCA) was performed on mean-centred data scaled to unit variance with MatLab software, version 7.4.0 (The MathWorks, Inc, Natick, MA, USA). Analyte relationships were visualized and studied using correlation networks (Weckwerth *et al.*, 2004; Schauer *et al.*, 2006; Carli *et al.*, 2009). In such networks, analytes (vertices) are connected with a link (edge) in a two-dimensional plane or three-dimensional space, such that their pairwise distances reflect their pairwise correlation coefficients when these coefficients exceed a given threshold. For these correlation networks, we used distances based on $1 -$ the absolute value of Spearman correlation coefficients (r) calculated for the three biological replicates of all tissue locations and developmental stages using MatLab (version 7.4.0). Bonferroni correction was used for the r significance threshold, but when the networks were too dense for interpretation at $P < 10^{-6}$ it was replaced by the more stringent threshold of $r > 0.90$ or $r < -0.90$. These relationships were visualized globally for all analytes using Arena3D (Pavlopoulos *et al.*, 2008) for network cartography with Fruchterman–Reingold algorithm. For this global network, in the rare cases that the same metabolite was determined by different analytical techniques, only absolute quantification data were retained. In order to partition the analytes into discrete groups of spatial and temporal patterns, we used a clustering approach. K-means clustering (MeV version 4.2) on the mean of the three biological replicates (data mean centred and reduced to unit variance and with distance based on correlation) grouped all significant analytes showing common trends. Several cluster numbers between eight and 15 were compared for K-means clustering and the 12-cluster grouping was chosen. For three relevant clusters, correlation networks cartography was done using Cytoscape software, version 6.2 (Shannon *et al.*, 2002; <http://www.cytoscape.org/>) with the spring-embedding algorithm. For volatile GC-MS and LC-QTOF-MS data of metabolites, informational redundancy among the unidentified analytes (e.g. fragments, isotopes or adducts from the same metabolite) has been decreased by clustering mass features during the data preprocessing step specific to each MS analytical strategy, as mentioned earlier. The possible remaining redundancy might have a low effect on the results of the correlation network cartography since mass signals from the same metabolites should follow a similar pattern. The heat map of analyte distribution according to stage and position was constructed using MeV, version 4.2.

Results

Metabolite and element profiles in fruit show dramatic temporal and spatial variation

Metabolite and mineral element profiles of different flesh sections were determined in fruit harvested at three stages: stage 1, just before the initiation of ripening; stage 2, early ripening; and stage 3, ripe fruit. For each fruit, five sections across the flesh, from outer or hypodermal mesocarp to inner mesocarp (Fig. 1), were separated and analysed using six complementary analytical technologies. $^1\text{H-NMR}$ and GC-MS (derivatized extracts) analyses were performed for polar primary metabolites, LC-PDA-FL for apolar isoprenoids, LC-MS for semipolar secondary metabolites, headspace GC-MS for volatile compounds and ICP-MS for mineral elements. This allowed the detection of 1932 analytes. Hereafter, the term ‘analyte’ will refer to one of the following: an unambiguously identified metabolite, a tentatively identified metabolite, an unidentified metabolite or a mineral element. Inherent in the different sample extracts and metabolomics technologies used, the amount of analytes detected and percentages of identified and quantified analytes varied between the platforms (Table S4). For example, the LC-MS platform provided relative concentrations of 1246 metabolites, of which 25 have so far been identified, whereas the $^1\text{H-NMR}$ platform provided absolute concentrations of 37 metabolites, of which 28 were identified. The analytical technologies were highly complementary: among the 197 identified compounds (see Tables S1, S2 for LC-MS and volatiles), < 20 were detected by more than one technology.

Analysis of variance was used after \log_e transformation to select analytes that showed significant differences ($P < 0.05$) related to developmental stage, flesh position or stage \times position interaction (Table S4). We compared the flesh sections throughout fruit development using PCA on the 1691 analytes that passed the ANOVA selection. The PCA scores (Fig. 2a) revealed that the composition of the five flesh sections differed at each stage of development. Indeed, the first principal component (PC1) clearly separated the samples of stage 3 from those of stages 1 and 2. For each stage, the sections followed parallel trajectories mostly along PC2 between sections 1 and 3 and along PC1 between sections 4 and 5. Examination of the loadings (Fig. 2b) suggested that the differences between stages and between sections each involved analytes detected by all the analytical technologies, as was confirmed by the heat map of the distributions of analytes (Fig. S1).

Global correlation network analysis reveals coregulation of metabolites between different chemical families

To obtain a global overview of the interanalyte associations, we employed Spearman correlation coefficients (r) between

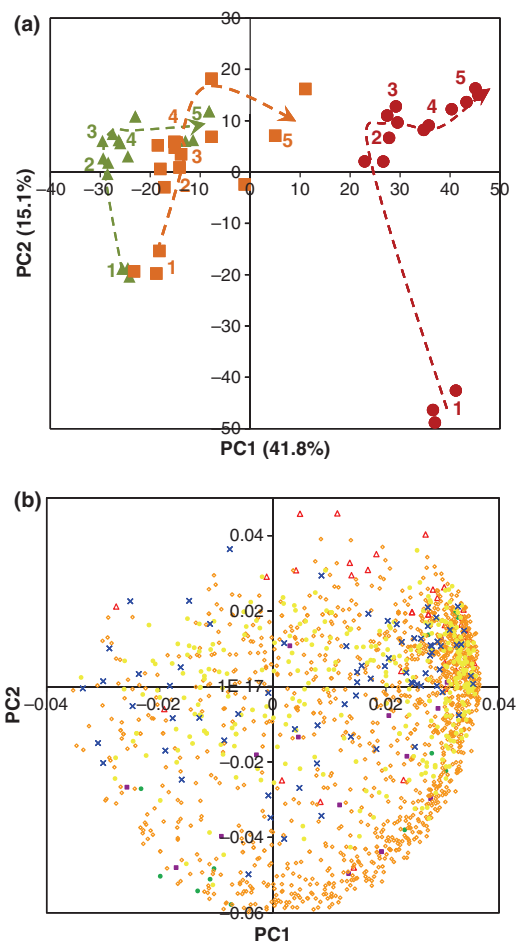


Fig. 2 Principal component analysis (PCA) of 1676 identified or unidentified metabolites measured by quantitative proton NMR spectroscopy ($^1\text{H-NMR}$, 37 metabolites), liquid chromatography coupled to photodiode array and fluorescence detection (LC-PDA-FL, 15 metabolites), LC-MS (1216 metabolites), GC-MS (76 polar metabolites and 332 volatiles) and 15 elements measured by inductively coupled plasma mass spectrometry (ICP-MS) in five radial sections from the flesh of melon fruit (1, outer; 5, inner; see Fig. 1) at three stages of development (1, youngest, green triangles; 2, orange squares; 3, oldest, red circles). (a) PCA scores plot of the first two principal components (PC1 and PC2). (b) PCA loadings plot. For each principal component, the loadings are indexed according to the corresponding analytical technology: $^1\text{H-NMR}$, red triangles; LC-PDA-FL, green circles; GC-MS, blue crosses; LC-MS, orange diamonds; GC-MS of volatiles, yellow diamonds; ICP-MS, purple squares).

the 1691 analytes selected after ANOVA. As the correlation network appeared unreadable at the $P < 10^{-6}$ significance threshold, we selected r coefficients with an absolute value > 0.90 ($P < 6 \times 10^{-11}$). This resulted in a network containing 715 analytes. We highlighted the connections between compound types using a layered network for visualization in three dimensions. The four layers corresponded to the following compound types: primary metabolites, nonvolatile secondary metabolites, volatiles and mineral elements. An

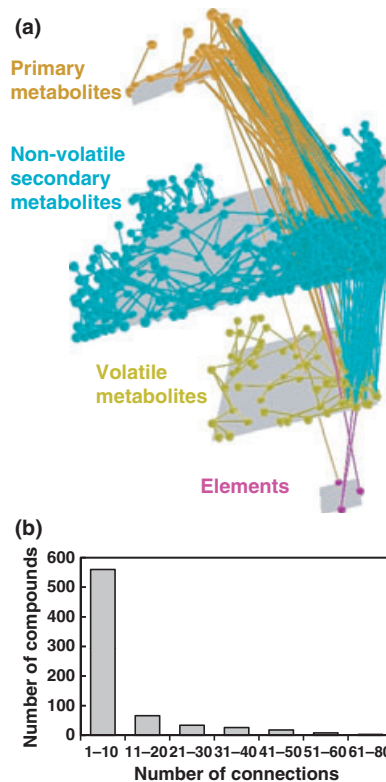


Fig. 3 Melon flesh correlation network based on Spearman r coefficients for 715 analytes (70 identified metabolites, 642 annotated metabolites characterized with retention time (RT) and m/z) and three elements, corresponding to analytes having correlation coefficients above the chosen $|r| > 0.90$ threshold (probability threshold of $P < 6 \times 10^{-11}$ after Bonferroni correction). Redundant metabolite determinations and unconnected analytes are not visualized. The measurements were classified into four analyte groups: primary metabolites (quantitative proton NMR spectroscopy, $^1\text{H-NMR}$; gas chromatography coupled with mass spectrometry, GC-MS), nonvolatile secondary metabolites (liquid chromatography coupled to photodiode array and fluorescence detection (LC-PDA-FL); liquid chromatography coupled to mass spectrometry LC-MS), volatile metabolites (headspace GC-MS) and elements (inductively coupled plasma mass spectrometry, ICP-MS). Correlations were calculated from data of three replicates of five sections from the fruit flesh at three stages of development. (a) Three-dimensional correlation network visualized using the Arena3D software. For each layer that corresponds to an analyte group, a network layout based on the within-layer analyte \times analyte correlations was performed. (b) Distribution of the number of network edges among the 715 analytes of the layered correlation network visualized in Fig. 2(a). The most highly connected analytes (hubs) are listed in Supporting Information, Table S3.

overview of the global network (Fig. 3a) revealed numerous connections between primary and nonvolatile secondary metabolites, as well as between nonvolatile secondary metabolites and volatiles. Only a few direct connections between primary metabolites and volatiles were observed. Most analytes were connected to up to 10 other analytes (Fig. 3b). Some parts of the network were very dense, consisting of 96

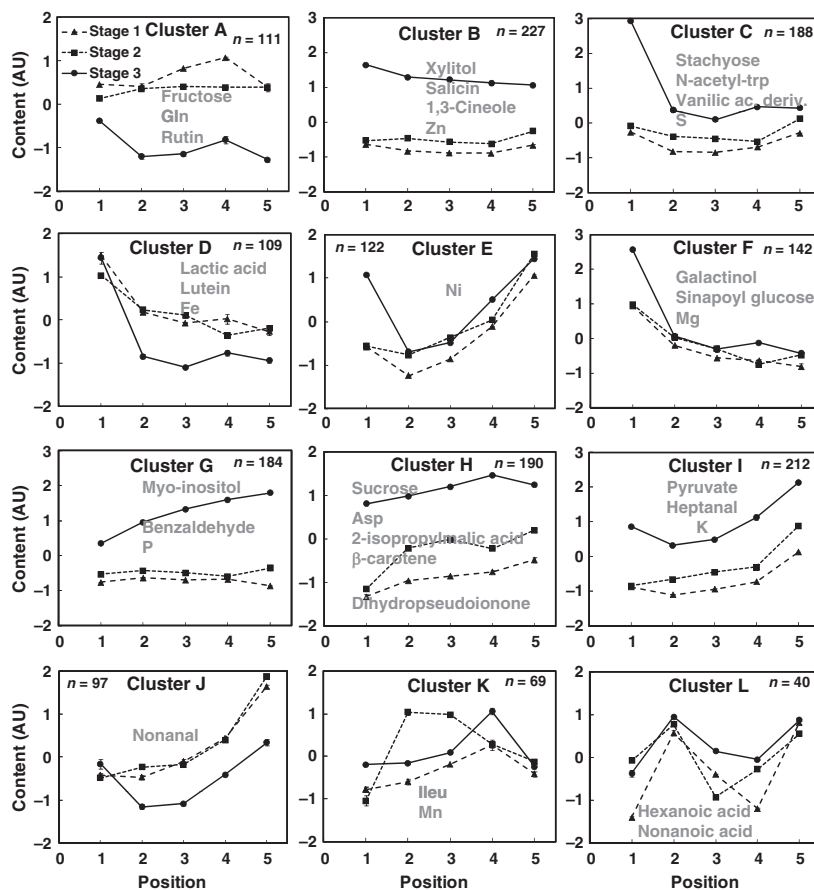


Fig. 4 Spatial distribution patterns of 1691 analytes in the flesh of melon fruit at three stages (1, triangles; 2, squares; 3, circles) of development. Twelve patterns were inferred through K-means clustering. Line graphs indicate the mean of all analytes in each cluster. Vertical bars represent the standard errors when these exceeded the symbol size. The number of analytes (n) in each cluster is reported. See Table 1 for the identified metabolites in each cluster. As examples, a number of key representative metabolites are given.

analytes, listed in Table S3, with 20 or more connections. These correspond to three primary metabolites (aspartic acid, sucrose and 2-isopropylmalic acid), a glutamine derivative, four nonvolatile secondary metabolites of the isoprenoid family (β -carotene, a β -carotene isomer, phytoene and a phytofluene isomer), one volatile compound (dihydropseudoionone, related to carotenoid metabolism), all listed along with their immediate neighbours in Table S3, and to 87 partially characterized semipolar compounds determined by LC-MS.

Clustering reveals compound groups changing according to developmental stage, position or both

To dissect the temporal and spatial analyte patterns, we used K-means clustering. This resulted in 12 analyte clusters (Fig. 4, Table 1) further classified into four groups. It is noticeable that of the 16 metabolites quantified by more than one technique, 13 were recovered in the same K-means cluster. The first group (clusters A–D) showed major temporal changes. The second group (clusters E–F) showed major spatial changes. The third group (clusters G–J) showed interactions of spatial and temporal changes. By contrast, the fourth group (clusters K–L) showed no clear trend. In summary, several analytes had higher concen-

trations in the outer mesocarp (section 1) than in the other flesh sections at one developmental stage or more. Several analytes had higher concentrations in the inner mesocarp (section 5) at several stages or only at stage 3. The major temporal and spatial trends highlighted with clustering are summarized on metabolic maps in Fig. S2.

Correlation networks of selected clusters reveal both expected and unexpected coregulated analytes

We selected three informative clusters presented in Fig. 4, to visualize their correlation networks: cluster F primarily shows only spatial changes, while clusters G and H show both temporal and spatial changes. For each cluster, Spearman correlation coefficients between analytes were calculated and used for visualization ($P < 10^{-6}$). Surprisingly, the connection density of these three clusters differed greatly: cluster H had the highest mean number of connections per node (33.5) followed by clusters G (8.4) and F (3.6). Cluster F contained analytes showing a decrease from section 1 to sections 4/5. The cluster F network (Fig. 5) was composed of 102 nodes with 365 significant connections. Of the 102 nodes, 93 were embedded in a unique network involving the primary metabolite galactinol and several known LC-MS analytes (including the ionone-

Table 1 Analyte composition of Fig. 4 clusters representing the spatial and developmental patterns of changes in melon flesh^a

| Clusters | Sugars/sugar alcohols | Organic acids | Fatty acids | Amino acids/amino compounds | Nonvolatile secondary metabolites | Volatiles | Elements |
|--|---|--|-------------------------------------|--|--|---|---------------------|
| Group 1 (major changes related with development) | | | | | | | |
| A | Fructose, glucose | Glyceric acid | | Glutamine | Benzylalcohol, a methyl-butanol-hexose-pentose, rutin, shikimic acid, violaxanthin-like compound 1 | 3-Octen-2-one | Pb |
| B | Threitol, xylitol | Isobutanoic acid, phosphoric acid monomethyl ester | Palmitic acid, 2-amino-stearic acid | | Coumaric acid hexose, salicin | Butyl acetate, hexyl acetate, benzylalcohol, butanoic acid, ethyl 2-methylbutanoate, 3-methylbutyl acetate, cinnamylacetate, β -damascenone, 1,8-cineole, α -ionene, propyl acetate, 3,6-nonadien-1-ol (E,Z)-2,3,3,5-Tetramethyloctane | |
| C | Stachyose | | | N-Acetyl-tryptophan | Acetyl(oxy)pentanoic acid, glucosylated chalcone-flavonone dimer-like, hydrocinnamic acid-hexose, hydroxy-dimethyl-decadienedioic acid-hexose, vanillic acid | | |
| D | | Lactic acid | | Ethanolamine | 3-neohesperidoside Chlorophyll A, chlorophyll B, lutein, methyl-butanol-hexose-pentose, violaxanthin-like compound 2, violaxanthin-like compound 3, vanillic acid (or a derivative) | Octanoic acid, 1-octen-3-ol | Ca Fe Mo |
| Group 2 (major changes related with tissue location) | | | | | | | |
| E | | | | | | | |
| F | Galactinol, galactose | Glycolic acid, malic acid | | Ornithine, ornithine-1,5-lactam | Benzylalcohol hexose-pentose, di-hydroxybenzoic acid hexose, ferulic acid hexose, sinapoyl glucose, tangshenoside I | | Ni B Cd Mg |
| Group 3 (interaction between developmental stage and tissue location) | | | | | | | |
| G | myo-Inositol, melibiose, trehalose ^b | Acetic acid, 3-hydroxy-butanoic acid, butyro-1,4-lactam, fumaric acid, malonic acid, succinic acid | | Alanine, amino-malonic acid, asparagine, glutamic acid, glutamine, glycine, methionine, phenylalanine, proline, pyroglutamic acid, serine, threonine, tryptophan, uracil, valine | Acetyl(oxy)pentanoic acid, <i>trans</i> -cinnamic acid, UDP-like compound | Ethyl acetate, methyl 2-methylbutanoate, benzaldehyde, 2-phenylethanol, 5,6,7,7a-tetrahydro-4,4,7 α -trimethyl-2(4H)-benzofuranone (R), 2,3-butanedioldiacetate, 3-methyl-2-butenyl acetate, ethyl 2-methyl-2butanoate, dimethyl disulfide, ethyl hexanoate, 3-hexenyl acetate, 2,3-dihydro-1,1,4,7-tetramethyl-1H-indene, ethyl 3-methylthiopropionate, neo-menthol | Cu P |

Table 1 (Continued)

| Clusters | Sugars/sugar alcohols | Organic acids | Fatty acids | Amino acids/amino compounds | Nonvolatile secondary metabolites | Volatiles | Elements |
|----------|---------------------------------|---|-------------|--|---|--|----------|
| H | Sucrose, trehalose ^c | Citric acid, formic acid, 2-isopropylmalic acid | | β -Alanine, aspartic acid, gamma-aminobutyric acid, glutamyl dopamine-like | Acetyl(oxy)pentanoic acid, adenosine-like compound, β -carotene, β -carotene-like compound 1, β -carotene-like compound 2, para-coumaric acid, coumaric acid-hexose, ferulic acid derivative, para-hydroxybenzoic acid hexose, phytoene, phytofluene, phytofluene-like compound | Phenylmethyl acetate, β -cyclocitral, dihydro- β -ionone, dihydropseudoionone, β -ionone | |
| I | | Itaconic acid, pyruvic acid | | Choline, trigonelline, tyrosine | Cumalic acid di-hexose, pantothenic acid hexose | Heptanal | K |
| J | | | | | | Nonanal | |

^aList of identified compounds that were quantified using proton NMR spectroscopy (¹H-NMR), liquid chromatography coupled to photodiode array and fluorescence detection (LC-PDA-FL), LC-MS, GC-MS or inductively coupled plasma mass spectrometry (ICP-MS) in terms of absolute or relative concentrations. The spatial and developmental consensus patterns of pool sizes were characterized using K-means clustering. The compounds in 10 of the 12 clusters in Fig. 4 are listed. Group 1 corresponds to the clusters showing major changes correlated with developmental stage and tissue location.

^bGC-MS-detected.

^c¹H-NMR-detected.

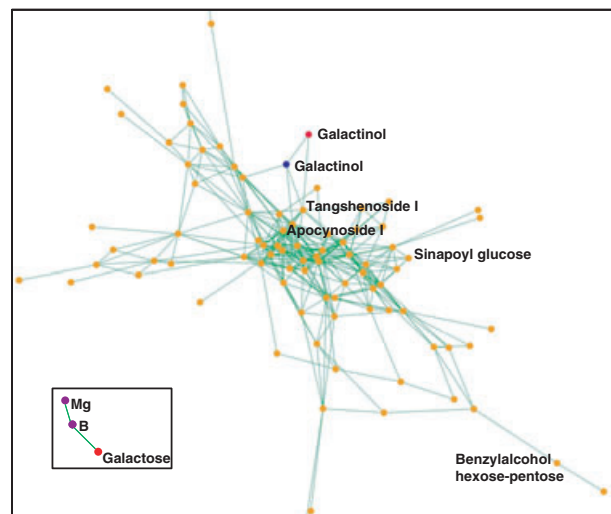


Fig. 5 Correlation network of one of the three most relevant clusters from Fig. 4. Spearman correlations of analytes were calculated with a probability threshold of $P < 10^{-6}$ after Bonferroni correction. The analyte \times analyte correlation network was visualized using Cytoscape software. Vertices are coloured according to the analytical technique: red, proton NMR spectroscopy (¹H-NMR); green, liquid chromatography coupled to photodiode array and fluorescence detection (LC-PDA-FL); orange, LC-MS; blue, GC-MS; purple, inductively coupled plasma mass spectrometry (ICP-MS). Correlation networks of the 142 analytes in cluster F. The insert represents the galactose network.

glucoside apocynoside I and the phenylpropanoids sinapoyl glucose and tangshenoside I) and many unknown ones. In addition, a small isolated network comprising Mg, B and galactose was recovered. Cluster H showed a simultaneous increase of analytes from sections 1 to 5 for each developmental stage. The cluster H network (Fig. 6a) was composed of 179 nodes with 5993 connections. Of the 179 nodes, 173 were embedded in a unique network, including the majority of LC-MS analytes (including a coumaric acid-hexoside, three other known phenolics, and numerous unidentified metabolites), sucrose, trehalose, aspartic acid, gamma-aminobutyric acid (GABA), β -alanine, 2-isopropylmalic acid, several isoprenoids and several volatiles, including four isoprenoid-derived volatiles. Cluster G showed temporal differences with a spatial gradient appearing at stage 3. The cluster G network (Fig. 6b) was composed of 161 nodes with 1359 connections. Of the 161 nodes, 157 were embedded in a unique network involving an interconnection of amino acids, organic acids and unknown LC-MS analytes, and a cluster of volatiles connected with metabolites detected by LC-MS. Cu was directly connected to fumaric acid and two unknown LC-MS analytes ($m/z = 597.166$, retention time (RT) = 10.82 and $m/z = 360.160$, RT = 8.31). Among the volatiles, benzaldehyde was directly connected to 11 other volatiles, while ethyl hexanoate was connected to alanine and serine.

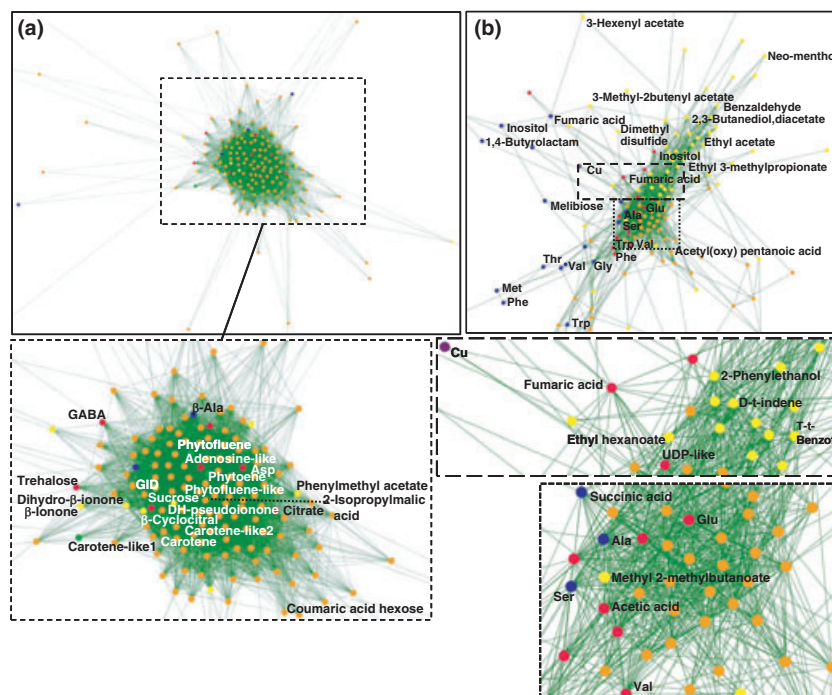


Fig. 6 Correlation networks of two of the three most relevant clusters from Fig. 4. Spearman correlations of analytes were calculated with a probability threshold of $P < 10^{-6}$ after Bonferroni correction. The analyte \times analyte correlation network was visualized using Cytoscape software. Vertices are coloured according to the analytical technique: red, proton NMR spectroscopy ($^1\text{H-NMR}$); green, liquid chromatography coupled to photodiode array and fluorescence detection (LC-PDA-FL); orange, LC-MS; blue, GC-MS; yellow, GC-MS of volatiles; purple, inductively coupled plasma mass spectrometry (ICP-MS). (a) Correlation network of the 190 analytes in cluster H (upper left); an annotated zoom-in of the most highly interconnected core of analytes is also presented (lower left). GID, glutamine derivative; DH-pseudoionone, dihydropseudoionone. (b) Correlation network of the 184 analytes in cluster G (upper right); zoom-in of parts of the most highly interconnected core of analytes are also presented (lower right). D-t-indene, 2,3-dihydro-1,1,4,7-tetramethyl-1H-indene; T-t-benzof., 5,6,7,7a-tetrahydro-4,4,7a-trimethyl-2(4H)-benzofuranone (R).

Discussion

Profiling by six platforms provided an unmatched comprehensive insight into the metabolome of the economically important crop, melon. The majority of the 1932 analytes detected changed during fruit development (Fig. S2a), demonstrating that metabolism is globally reprogrammed during ripening. Furthermore, the highly correlative nature of these analytes, forming a highly integrated network, emphasizes the growing need for system-oriented approaches to understand such complex processes. Consequently, future breeding efforts should strive to understand the molecular and regulatory mechanisms underlying these global metabolome patterns.

Extensive metabolite gradients, as identified here (Fig. S2b), clearly define the four-dimensional nature of fruit ripening. Anatomical differences may play a role in the nonuniform ripening progression across the fruit. The distribution of vascular bundles determines the local concentration of sugars or K delivered through the phloem sap to the fruit. This mechanism may be reflected, for instance, by the presence of galactinol in the outer mesocarp (Fiehn, 2003). The production of phytohormones by the seeds and their diffusion

gradients across the melon fruit flesh may also trigger metabolic changes as suggested for auxin in tomato fruit (Lemaire-Chamley *et al.*, 2005). Besides, the fruit primary metabolism is highly dependent on oxygen gradients, which can lead to hypoxia in the centre of the fruit (Sugiyama, 1999; Lester, 2008; Biais *et al.*, 2009, 2010). Our study reflects such effects through the increase in sucrose, alanine, valine, GABA and acetic acid towards the inner mesocarp. For secondary metabolites, the gradients caused by intercellular translocation need to be considered (Kutchan, 2005). By contrast, mineral elements depend on the distribution and expression pattern of ion transporters (Davies *et al.*, 2006; Karley & White, 2009), the balance between xylem and phloem long-distance transport and the sites of ion complex formation (Conn & Gilliam, 2010). Future breeding efforts towards a more homogenous melon fruit may include selection towards more homogenous tissue vascularization and possibly seedless fruits.

In a recent omics study in yeast, changes in metabolite concentrations have been clearly shown to reflect the metabolic pathway distance (Walther *et al.*, 2010). Furthermore, metabolite concentrations proved more reliable in this regard than did transcript abundance. Our study includes a

rich resource to develop such insights beyond the coregulation of metabolic pathways demonstrated using the stages of tomato fruit development (Carrari *et al.*, 2006). For example, correlations within pathways were observed for the amino acids originating from oxaloacetate, rendering the root of this pathway branch a potential key target for breeding efforts. We also detected an interaction between amino acid biosynthesis and phenolic compounds in agreement with findings in the strawberry fruit (Fait *et al.*, 2008). Most important for future flavour design in melon were interactions between primary metabolism and the volatile bouquet. The aroma volatiles in cantaloupe melons are a complex mixture of chemically diverse esters, aldehydes, alcohols and sulphur compounds (Obando-Ulloa *et al.*, 2008; Schwab *et al.*, 2008). We demonstrated a close link between alanine and serine and the production of ethyl hexanoate. This finding justifies focusing efforts towards quality improvement on this specific path among the many potential associations of volatile esters originating from the branched alkyl chains of amino acid metabolism (Gonda *et al.*, 2010). Palmitic acid and 2-amino-stearic acid had a pattern similar to several volatiles, including butyl acetate and hexyl acetate, pointing to the importance of aliphatic ester and alcohol production from free fatty acids. Six isoprenoids, including β -carotene, correlated significantly to β -cyclocitral, β -ionone, dihydro- β -ionone and dihydropseudoionone, reflecting not only their known synthesis from the degradation of carotenoids (Schwab *et al.*, 2008) but also the clear dependence of products and precursors in melon fruit tissue. Finally, the cluster containing methionine also contained two other sulphur-containing compounds. Therefore, our study reaches beyond confirmation of known biosynthetic pathways having multiple connections between primary metabolism and secondary products linked to flavour. Importantly, we not only demonstrate novel interactions with as yet unknown flavour components but also confirm which of the many possible pathway interactions are indeed expressed in melon fruit. Such clear spatially or developmentally supported product and precursor interactions should help to direct future evidence-based breeding efforts in melon.

Besides direct enzymatic links between metabolites, coregulation also results from the regulatory control of metabolism, which is largely not understood beyond the key aspects of central metabolism. Indeed, correlation networks in melon fruit have revealed several so-called 'hub' metabolites closely associated to a multitude of other metabolites. These metabolites may be key to understanding as yet unknown metabolic components or signalling mechanisms. Sucrose, as the most obvious hub metabolite in fruit development, supports the hub concept. This sugar is a main intermediate of carbohydrate metabolism and has been characterized as a signalling metabolite (Rolland *et al.*, 2006). Likewise, aspartic acid and a glutamine derivative appear as two new hub metabolites in melon fruit. Besides being one

of the main amino acids transported in cucurbit phloem (Fiehn, 2003), aspartic acid occupies a pivotal position in amino acid metabolism and pyrimidine biosynthesis. Considering the dual function of N-transport metabolites and their potential as signalling molecules relevant for the C : N balance in fruit tissue (Mounet *et al.*, 2009), the hub metabolite concept visualizes the specific importance of aspartic acid in melon fruit development. Interestingly, glutamic acid has been recently proposed to have signalling properties in plants (Forde & Lea, 2007). Furthermore, 2-isopropylmalic acid was the network hub with the highest number of connections in our study. This metabolite is an intermediate of leucine biosynthesis (Hagelstein & Schultz, 1993), which may be a key precursor of aldehydes and alcohols present in melon fruit (Schwab *et al.*, 2008; Gonda *et al.*, 2010). Therefore we hypothesize that a higher synthesis capacity for 2-isopropylmalic acid is a potential biotechnological target for the improvement of melon fruit organoleptic quality. In addition, four nonvolatile isoprenoids and one carotenoid-derived volatile (Simkin *et al.*, 2004) also appeared as hub metabolites, suggesting a signalling role in melon as these detected hubs represent, in part, oxidative cleavage of carotenoids which have been implied as signalling molecules in other plant tissues (Auldridge *et al.*, 2006; Tsuchiya & McCourt, 2009).

The associations of mineral concentrations with metabolite patterns during spatial and developmental changes are novel. Ca, iron (Fe) and molybdenum (Mo) contents reflected those of a set of isoprenoids. As a proof of concept we confirmed the expected association between Fe and chlorophyll (Briat *et al.*, 2007). In addition, K, a known activator of phosphofructokinase and pyruvate kinase (Armengaud *et al.*, 2009; Maathuis, 2009), was highly correlated with pyruvic acid. We now also have clear evidence that boron (B) is correlated to phenolic constituents in melon. Therefore, B deficiency needs to be considered in melon cultivation regarding overall phenolics composition (Camacho-Cristóbal *et al.*, 2008). B also exhibited a pattern highly similar to galactose and galactinol. This suggests a possible link with raffinose or cell wall metabolism and a role of B-galactinol complexes as shuttles for B redistribution from the vegetative parts to the fruit (Camacho-Cristóbal *et al.*, 2008). Phosphorus (P) correlated strongly with inositol in melon flesh. The role of inositol biosynthesis in phosphate storage may need to be extended from seeds to fruit flesh but currently remains elusive in these tissues. Finally, Copper (Cu) proved also to be a major hub element in melon fruit. Cu was associated with 14 amino compounds including proline. The known Cu-complexing property of amino compounds (Sharma & Dietz, 2006) may be seen as a major caveat for breeding or engineering melon fruit towards higher Nitrogen (N) or amino acid content. Such efforts should be accompanied by monitoring the effects on heavy metal accumulation in melon fruit.

To our knowledge this in-depth metabolome analysis of melon, as an example of fleshy fruits, is unprecedented in terms of the range and combination of analytical techniques. The proposed concept of characterizing and defining 'hub' metabolites is supported in many aspects. Such analyses of metabolic association networks helped to pinpoint the specific relevance of certain known analyte interactions in breeding for nutritionally important plant organs, but also revealed unexpected interactions such as mineral element–metabolite interactions. Metabolome profiles may ensure that targeted breeding efforts for improved quality retain focus through aspects that were not pre-conceived. Future studies will exploit the vast natural variation in melon and search for single nucleotide polymorphism markers specifically affecting the hub metabolites, flavour components and mineral elements identified here.

Acknowledgements

We thank Dr A. A. Schaffer for valuable comments, Dr C. Cheniclet for help with Fig. 2, D. Jacob for developing the MeRy-B database, S. Bochu and F. Leix-Henry (CEFEL, France) for providing the fruits and I. Quintana for uploading NMR spectra into MeRy-B. This work was supported by the EU FP6 project META-PHOR (grant no. FOOD-CT-2006-036220). R.D.H., R.M. and R.C.H. de V. acknowledge additional financial support from the Netherlands Genomics Initiative via the Centre for BioSystems Genomics and the Netherlands Metabolomics Centre.

References

- Aharoni A, de Vos CHR, Verhoeven HA, Maliepaard CA, Kruppa G, Bino RJ, Goodenow DB. 2002. Nontargeted metabolome analysis by use of Fourier transform ion cyclotron mass spectrometry. *OMICS: A Journal of Integrative Biology* 6: 217–234.
- Allwood JW, Erban A, de Koning S, Dunn WB, Luedemann A, Lommen A, Kay L, Löscher R, Kopka J, Goodacre R. 2009. Inter-laboratory reproducibility of fast gas chromatography – electron impact – time of flight mass spectrometry (GC-EI-TOF/MS) based plant metabolomics. *Metabolomics* 5: 479–496.
- Armengaud P, Sulpice R, Miller AJ, Stitt M, Amtmann A, Gibon Y. 2009. Multilevel analysis of primary metabolism provides new insights into the role of potassium nutrition for glycolysis and nitrogen assimilation in Arabidopsis roots. *Plant Physiology* 150: 772–785.
- Auldridge ME, McCarty DR, Klee HJ. 2006. Plant carotenoid cleavage oxygenases and their apocarotenoid products. *Current Opinion in Plant Biology* 9: 315–321.
- Beaulieu JC, Grimm CC. 2001. Identification of volatile compounds in cantaloupe at various developmental stages using solid phase micro-extraction. *Journal of Agricultural and Food Chemistry* 49: 1345–1352.
- Bedair M, Sumner LW. 2008. Current and emerging mass-spectrometry technologies for metabolomics. *Trends in Analytical Chemistry* 27: 238–250.
- Biais B, Allwood JW, Deborde C, Xu Y, Maucourt M, Beauvoit B, Dunn WB, Jacob D, Goodacre R, Rolin D *et al.* 2009. ¹H-NMR, GC-EI-TOF-MS and data set correlation for fruit metabolomics, application to spatial metabolite analysis in melon. *Analytical Chemistry* 81: 2884–2894.
- Biais B, Beauvoit B, Allwood JW, Deborde C, Maucourt M, Goodacre R, Rolin D, Moing A. 2010. Metabolic acclimation to hypoxia revealed by metabolite gradients in melon fruit. *Journal of Plant Physiology* 167: 242–245.
- Bino RJ, de Vos CHR, Lieberman M, Hall RD, Bovy A, Jonker HH, Tikunov Y, Lommen A, Moco S, Levin I. 2005. The light-hyperresponsive *high pigment-2^{hg}* mutation of tomato: alterations in the fruit metabolome. *New Phytologist* 166: 427–438.
- Briat J-F, Curie C, Gaymard F. 2007. Iron utilization and metabolism in plants. *Current Opinion in Plant Biology* 10: 276–282.
- Burger Y, Schaffer AA. 2007. The contribution of sucrose metabolism enzymes to sucrose accumulation in *Cucumis melo*. *Journal of the American Society for Horticultural Science* 132: 704–712.
- Camacho-Cristóbal JJ, Rexach J, González-Fontes A. 2008. Boron in plants: deficiency and toxicity. *Journal of Integrative Plant Biology* 50: 1247–1255.
- Carli P, Arima S, Fogliano V, Tardella L, Frusciantè L, Ercolano MR. 2009. Use of network analysis to capture key traits affecting tomato organoleptic quality. *Journal of Experimental Botany* 60: 3379–3386.
- Carrari F, Baxter C, Usadel B, Urbanczyk-Wochniak E, Zanon MI, Nunes-Nesi A, Nikiforova V, Centero D, Ratzka A, Pauly M *et al.* 2006. Integrated analysis of metabolite and transcript levels reveals the metabolic shifts that underlie tomato fruit development and highlight regulatory aspects of metabolic network behavior. *Plant Physiology* 142: 1380–1396.
- Conn S, Gilliam M. 2010. Comparative physiology of elemental distribution in plants. *Annals of Botany* 105: 1081–1102.
- Cuevas HE, Staub JE, Simon PW, Zalapa JE, McCreight JD. 2008. Mapping of genetic loci that regulate quantity of beta-carotene in fruit of US Western Shipping melon (*Cucumis melo* L.). *Theoretical and Applied Genetics* 117: 1345–1359.
- Davies C, Shin R, Liu W, Thomas MR, Schachtman DP. 2006. Transporters expressed during grape berry (*Vitis vinifera* L.) development are associated with an increase in berry size and berry potassium accumulation. *Journal of Experimental Botany* 57: 3209–3216.
- Fait A, Hanhineva K, Beleggia R, Dai N, Rogachev I, Nikiforova JV, Fernie AR, Aharoni A. 2008. Reconfiguration of the achene and receptacle metabolic networks during strawberry fruit development. *Plant Physiology* 148: 730–750.
- Fernie AR, Schauer N. 2009. Metabolomics-assisted breeding: a viable option for crop improvement? *Trends in Genetics* 25: 39–48.
- Fiehn O. 2003. Metabolic networks of *Cucurbita maxima* phloem. *Phytochemistry* 62: 875–886.
- Fiehn O, Kopka J, Dormann P, Altmann T, Trethewey RN, Willmitzer L. 2000. Metabolite profiling for plant functional genomics. *Nature Biotechnology* 18: 1157–1161.
- Forde BG, Lea PJ. 2007. Glutamate in plants: metabolism, regulation, and signalling. *Journal of Experimental Botany* 58: 2339–2358.
- Gillaspy G, Ben-David H, Gruissem W. 1993. Fruits: a developmental perspective. *Plant Cell* 5: 1439–1451.
- Gonda I, Bar E, Portnoy V, Lev S, Burger J, Schaffer AA, Tadmor Y, Gepstein S, Giovannoni JJ, Katzir N *et al.* 2010. Branched-chain and aromatic amino acid catabolism into aroma volatiles in *Cucumis melo* L. fruit. *Journal of Experimental Botany* 61: 1111–1123.
- Hagelstein P, Schultz G. 1993. Leucine synthesis in spinach chloroplasts: partial characterization of 2-isopropylmalate synthase. *Biological Chemistry Hoppe-Seyler* 374: 1105–1108.
- Hall RD, Brouwer ID, Fitzgerald MA. 2008. Plant metabolomics and its potential application for human nutrition. *Physiologia Plantarum* 132: 162–175.

- Hanhineva K, Rogachev I, Kokko H, Mintz-Oron S, Venger I, Karenlampi S, Aharoni A. 2008. Non-targeted analysis of spatial metabolite composition in strawberry (*Fragaria × ananassa*) flowers. *Phytochemistry* 69: 2463–2481.
- Hansen TH, Laursen KH, Persson DP, Pedas P, Husted S, Schjoerring JK. 2009. Micro-scaled high-throughput digestion of plant tissue samples for multi-elemental analysis. *Plant Methods* 5 doi:10.1186/1746-4811-5-12.
- Hirai MY, Sugiyama K, Sawada Y, Tohge T, Obayashi T, Suzuki A, Araki R, Sakurai N, Suzuki H, Aoki K *et al.* 2007. Omics-based identification of *Arabidopsis* Myb transcription factors regulating aliphatic glucosinolate biosynthesis. *Proceedings of the National Academy of Sciences, USA* 104: 6478–6483.
- Hummel J, Strehmel N, Selbig J, Walther D, Kopka J. 2010. Decision tree supported substructure prediction of metabolites from GC-MS profiles. *Metabolomics* 6: 322–333.
- Karley AJ, White PJ. 2009. Moving cationic minerals to edible tissues: potassium, magnesium, calcium. *Current Opinion in Plant Biology* 12: 291–298.
- Kerr G, Ruskin HJ, Crane M, Doolan P. 2008. Techniques for clustering gene expression data. *Computers in Biology and Medicine* 38: 283–293.
- Kopka J, Schauer N, Krueger S, Birkemeyer C, Usadel B, Bergmuller E, Dormann P, Weckwerth W, Gibon Y, Stitt M *et al.* 2005. GMD@CSB.DB: the Golm metabolome database. *Bioinformatics* 21: 1635–1638.
- Kutchan TM. 2005. A role for intra- and intercellular translocation in natural product biosynthesis. *Current Opinion in Plant Biology* 8: 292–300.
- Laursen KH, Hansen TH, Persson DP, Schjoerring JK, Husted S. 2009. Multi-elemental fingerprinting of plant tissue by semi-quantitative ICP-MS and chemometrics. *Journal of Analytical Atomic Spectrometry* 24: 1198–1207.
- Lemaire-Chamley M, Petit J, Garcia V, Just D, Baldet P, Germain V, Fagard M, Mouassite M, Cheniclet C, Rothan C. 2005. Changes in transcriptional profiles are associated with early fruit tissue specialization in tomato. *Plant Physiology* 139: 750–769.
- Lester GE. 2008. Antioxidant, sugar, mineral, and phytonutrient concentrations across edible fruit tissues of orange-fleshed honeydew melon (*Cucumis melo* L.). *Journal of Agricultural and Food Chemistry* 56: 3694–3698.
- Liscic J, Schauer N, Kopka J, Willmitzer L, Fernie AR. 2006. Gas chromatography mass spectrometry-based metabolite profiling in plants. *Nature Protocols* 1: 387–396.
- Lommen A. 2009. MetAlign: interface-driven, versatile metabolomics tool for hyphenated full-scan mass spectrometry data preprocessing. *Analytical Chemistry* 81: 3079–3086.
- Luedemann A, Strassburg K, Erban A, Kopka J. 2008. TagFinder for the quantitative analysis of gas chromatography-mass spectrometry (GC-MS)-based metabolite profiling experiments. *Bioinformatics* 24: 732–737.
- Maathuis FJM. 2009. Physiological functions of mineral macronutrients. *Current Opinion in Plant Biology* 12: 250–258.
- Martin-Diana AB, Rico D, Frias JM, Barat JM, Henehan GTM, Barry-Ryan C. 2007. Calcium for extending the shelf life of fresh whole and minimally processed fruits and vegetables: a review. *Trends in Food Science & Technology* 18: 210–218.
- Mintz-Oron S, Mandel T, Rogachev I, Feldberg L, Lotan O, Yativ M, Wang Z, Jetter R, Venger I, Adato A *et al.* 2008. Gene expression and metabolism in tomato fruit surface tissues. *Plant Physiology* 147: 823–851.
- Mounet F, Lemaire-Chamley M, Maucourt M, Cabasson C, Giraudel JL, Deborde C, Lessire R, Gallusci P, Bertrand A, Gaudillere M *et al.* 2007. Quantitative metabolic profiles of tomato flesh and seeds during fruit development: complementary analysis with ANN and PCA. *Metabolomics* 3: 273–288.
- Mounet F, Moing A, Garcia V, Petit J, Maucourt M, Deborde C, Bernillon S, Le Gall G, Colquhoun I, Defernez M *et al.* 2009. Gene and metabolite regulatory network analysis of early developing fruit tissues highlights new candidate genes for the control of tomato fruit composition and development. *Plant Physiology* 149: 1505–1528.
- Nikiforova VJ, Willmitzer L. 2007. Network visualization and network analysis. In: Baginsky S, Fernie AR, eds. *Plant systems biology*. Basel, Switzerland: Birkhäuser, *Experientia Supplementum* 97: 245–275.
- Obando-Ulloa JM, Moreno E, Garcia-Mas J, Nicolai B, Lammertyn J, Monforte AJ, Fernandez-Trujillo JP. 2008. Climacteric or non-climacteric behavior in melon fruit – 1. Aroma volatiles. *Postharvest Biology and Technology* 49: 27–37.
- Pavlopoulos G, O'Donoghue S, Satagopam V, Soldatos T, Pafilis E, Schneider R. 2008. Arena3D: visualization of biological networks in 3D. *BMC Systems Biology* 2 doi:10.1186/1752-0509-2-104.
- Rolland F, Baena-Gonzalez E, Sheen J. 2006. Sugar sensing and signaling in plants: conserved and novel mechanisms. *Annual Review of Plant Biology* 57: 675–709.
- Saeed AI, Sharov V, White J, Li J, Liang W, Bhagabati N, Braisted J, Klapa M, Currier T, Thiagarajan M *et al.* 2003. TM4: a free, open-source system for microarray data management and analysis. *BioTechniques* 34: 374–378.
- Schauer N, Semel Y, Roessner U, Gur A, Balbo I, Carrari F, Pleban T, Perez-Melis A, Bruedigam C, Kopka J *et al.* 2006. Comprehensive metabolic profiling and phenotyping of interspecific introgression lines for tomato improvement. *Nature Biotechnology* 24: 447–454.
- Schwab W, Davidovich-Rikanati R, Lewinsohn E. 2008. Biosynthesis of plant-derived flavor compounds. *Plant Journal* 54: 712–732.
- Shannon P, Markiel A, Ozier O, Baliga NS, Wang JT, Ramage D, Amin N, Schwikowski B, Ideker T. 2002. Cytoscape: a software environment for integrated models of biomolecular interaction networks. *Proceedings of the 3rd International Conference on Systems Biology 2002*. Stockholm, Sweden, 2498–2504.
- Sharma SS, Dietz KJ. 2006. The significance of amino acids and amino acid-derived molecules in plant responses and adaptation to heavy metal stress. *Journal of Experimental Botany* 57: 711–726.
- Simkin AJ, Schwartz SH, Aldridge M, Taylor MG, Klee HJ. 2004. The tomato *carotenoid cleavage dioxygenase 1* genes contribute to the formation of the flavor volatiles β-ionone, pseudoionone, and geranylacetone. *Plant Journal* 40: 882–892.
- Smith CA, Want EJ, O'Maille G, Abagyan R, Siuzdak G. 2006. XCMS: processing mass spectrometry data for metabolite profiling using nonlinear peak alignment, matching, and identification. *Analytical Chemistry* 78: 779–787.
- Strehmel N, Hummel J, Erban A, Strassburg K, Kopka J. 2008. Retention index thresholds for compound matching in GC-MS metabolite profiling. *Journal of Chromatography B-Analytical Technologies in the Biomedical and Life Sciences* 871: 182–190.
- Sugiyama J. 1999. Visualization of sugar content in the flesh of a melon by near-infrared imaging. *Journal of Agricultural and Food Chemistry* 47: 2715–2718.
- Tikunov Y, Lommen A, de Vos CHR, Verhoeven HA, Bino RJ, Hall RD, Bovy AG. 2005. A novel approach for nontargeted data analysis for metabolomics. Large-scale profiling of tomato fruit volatiles. *Plant Physiology* 139: 1125–1137.
- Tsuchiya Y, McCourt P. 2009. Strigolactones: a new hormone with a past. *Current Opinion in Plant Biology* 12: 556–561.
- Verhoeven HA, Jonker H, de Vos RCH, Hall RD. 2011. Solid-phase micro-extraction (SPME) GC-MS analysis of natural volatile components in melon and rice. In: Hardy NG, Hall RD, eds. *Plant metabolomics methods*. Ithaca, NY, USA: Humana Press, in press.

- Walther D, Strassburg K, Durek P, Kopka J. 2010. Metabolic pathway relationships revealed by an integrative analysis of the transcriptional and metabolic temperature stress-response dynamics in yeast. *OMICS: A Journal of Integrative Biology* 14: 261–274.
- Weckwerth W, Loureiro ME, Wenzel K, Fiehn O. 2004. Differential metabolic networks unravel the effects of silent plant phenotypes. *Proceedings of the National Academy of Sciences, USA* 101: 7809–7814.
- White PJ, Broadley MR. 2003. Calcium in plants. *Annals of Botany* 92: 487–511.

Supporting Information

Additional supporting information may be found in the online version of this article.

Fig. S1 Visualization of analyte distribution in melon flesh using heat maps.

Fig. S2 Summary of the major developmental (a) or spatial (b) changes in relative or absolute concentrations of metabolites and mineral elements in melon fruits indicated on simplified metabolic maps.

Table S1 List of metabolites putatively identified in melon extracts by LC-QTOF-MS analysis

Table S2 List of volatile metabolites putatively identified in melon extracts by GC-MS analysis

Table S3 List of the 96 identified and partially characterized hub metabolites in the correlation network presented in Fig. 3

Table S4 Number of analytes and identified metabolites and elements, issued for each analytical technology, in melon extracts before and after the ANOVA analysis

Please note: Wiley-Blackwell are not responsible for the content or functionality of any supporting information supplied by the authors. Any queries (other than missing material) should be directed to the *New Phytologist* Central Office.